# ATLAS

P. Albicocco, M. Antonelli (Resp.), C. Arcangeletti (Ass. Ric.),
M. Battisti (Tech.), M.M. Beretta, B. Buadze, E. Capitolo (Tech.),
G. Capoccia (Ass. Ric.), G. Cesarini (Ass. Ric.), V. Chiarella,
Z. Chubinidze (Ass. Ric.), A. Croce (Tech.), E. Dane',
L. Gangadze, S. Lauciani (Tech.), C. Ligi, A. Martini, G. Mancini,
C. Paraskevopoulos (Borsa Stranieri), G. Pileggi (Tech.), B. Ponzio (Tech.),
F. Rosatelli (Tech.), A. Sansoni, M. Testa,
S. Tomassini, L. Vannoli (Ass. Ric.), E. Vilucchi.

March 14, 2024

# 1 Introduction

In the 2019-2021 Long Shut Down 2, ATLAS took the opportunity to upgrade the forward part of the Muon Spectrometer with new tecnology detectors such as MicroMegas, replacing the old Small Wheels with New Small Wheels (NSW).
Our group contributed with leading roles to the construction, integration and commisisoning of the MM detectors for the NSW and continued contributing significantly in the analysis in the $H \to ZZ \to 4\ell$ decay channel.
These contributions have been made possible also thanks to the reliability and the tools available on the technical team and of the LNF Tier2 approved by the INFN.
In parallel, we are deeply involved in the main upgrade Phase II activity concerning the Inner Tracker (ITk) upgrade.

# 2 Tier2

The Frascati group gives a significant contribution also to the ATLAS distributed computing, managing one of the experiment's Tier2s. The data center that hosts the Tier2 is a facility of the Laboratories where also computing activities related to different INFN experiments and projects are implemented. Please refer to the "Scientific Computing" report for the description of all the projects implemented in this infrastructure.
**Responsabilities:**

- Global responsabilities: (E. Vilucchi) co-responsible of the Virtual Organization Management for ATLAS
- Local responsabilities:
- 1. Within the Piano Nazionale di Ripresa e Resilienza (PNRR 2022): (E. Vilucchi) local responsible of ICSCS0, Italian Center for Super Computing, for the Laboratori Nazionali di Frascati of INFN.
- 2. Within the Project CIR01 00011 I.Bi.S.Co. - Infrastructure for Big data and Scientific Computing: (E. Vilucchi) scientific coordinator for the Laboratori Nazionali di Frascati of INFN.
- 3. Within the Project I.Bi.S.Co. for the PON-DHTCS: (E. Vilucchi) scientific responsible of the project for the LNF Tier2 improvement.

# 3 Higgs properties

The Higgs boson is the keystone particle of the Standard Model (SM) and its existence explains the massive nature of matter.
The Large Hadron Collider, located at CERN laboratory in Geneva, is the largest particle accelerator in the world and it is designed to allow the search for new processes at the TeV scale. At the LHC, the Higgs boson can be produced via different processes. The gluon fusion (ggF) process represents the main production mode, followed by the vector-boson fusion production (VBF), vector-boson associated production (VH) and the associated production with a top quark pairs (ttH). The Higgs boson decays into pairs of fermions or bosons, and it can be detected through the different final states in several decay channels. The most sensitive decay channels at LHC are: $H \to W^+W^-$, $H \to \gamma\gamma$ and $H \to ZZ^* \to 4l$.
The first measurements performed during the Run1 at the Large Hadron Collider (LHC) allowed for the discovery of the Higgs boson, announced by the ATLAS [4] and CMS collaborations [5] in July 2012. Since that moment, one of the main goal of the ATLAS experiment has been to study the Higgs boson properties.
The activity of the ATLAS LNF group is focused on the study of the Higgs boson properties in the $H \to ZZ^* \to 4l$ decay channel. This channel is one of the best channel to study the Higgs boson properties, due to the high signal-background ratio ($\sim 2$) and to the clear signature, despite the low Branching Ratio ($(1.25 \pm 0.03) \times 10^{-4}$.
In the Run 2 the improvements implemented in the analysis of this channel together with the enhancement of the statistics up to 139 fb$^{-1}$ have allowed more precise measurements of the Higgs boson properties: couplings, differential cross section, mass, width and spin/CP, increasing the sensitive to possible Beyond Standard Model (BSM) effects. The LNF analysis team is involved into the study of the CP properties of the Higgs boson in this decay channel using the Run 2 dataset, as well as into the coordination of the combined mass measurement Run1 + Run2 between $H \to ZZ^* \to 4l$ and $H \to \gamma\gamma$ decay channels.
From July 2022 the Run 3 on LHC started with proton-proton collisions at 13.6 TeV, collecting an integrated luminosity of 30.7 fb$^{-1}$. One of the first measurement at 13.6 TeV that will be provided by ATLAS is the fiducial cross section measurement of the $H \to ZZ^* \to 4l$ decay channel, in which the LNF team cover a coordinating role.

## 3.1 Test of CP-invariance of the Higgs boson in Vector Boson Production and its decay to Four Leptons [1]

The spin-parity ($J^P$) of the Higgs boson is predicted to be $0^+$ by the Standard Model[1]. Any sign of CP-violation in the production or decay of the Higgs

[1]In the following, only the $J^P$ label is used to indicate the spin and CP quantum numbers.

boson would therefore be an unambiguous indication of Beyond the Standard Model phenomena (BSM).
With 25 fb$^{-1}$ of proton-proton collision data collected from the LHC with a centre-of-mass energy, $\sqrt{s}$, of 7 and 8 TeV, the ATLAS and CMS experiments excluded the pure spin-parity states $0^-$, $1^+$, $1^-$, $2^+$ and $2^-$ at more than 99% confidence level based on the observed Higgs boson decays ($\gamma\gamma, ZZ, WW$). Run 1 results provided the first limits on a possible CP-odd contribution to Higgs boson to vector boson couplings ($HVV$) in Higgs boson decays. With an increased integrated luminosity of 139 fb$^{-1}$ of LHC collisions at $\sqrt{s} = 13$ TeV, an order of magnitude more Higgs boson candidates were collected. Constraints on CP-invariance were tightened for the $HVV$ couplings and extended to Higgs Yukawa couplings to fermions. For the $H \to ZZ^* \to 4\ell$ channel ($\ell = e, \mu$), constraints on both CP-even and CP-odd BSM couplings have been set with 139 fb$^{-1}$ at $\sqrt{s} = 13$ TeV for Higgs boson production cross section measurements, by comparing observations with SM expectations [6]. However, potential deviations of the Higgs boson production cross sections could be explained by either a CP-even or CP-odd BSM coupling, and would not distinguish between them. The present analysis searches for a visible CP-odd effect in VBF production and the $H \to ZZ^* \to 4\ell$ decay by employing *optimal observables* [7] with 139 fb$^{-1}$ of data collected at $\sqrt{s} = 13$ TeV by the ATLAS detector. About 10 events in a VBF production phase space and about 200 Higgs bosons decaying to four leptons are expected in this sample. The optimal observables are constructed from matrix elements of the Standard Model Effective Field Theory (SMEFT) [8], a specific formalism of an Effective Field Theory (EFT). The optimal observables are formed from the squared amplitude of the interference term between the SM matrix element and a dimension six operator matrix element of the SMEFT Lagrangian $\mathcal{OO} = \frac{2\Re(\mathcal{M}^*_{SM}\mathcal{M}_{BSM})}{|\mathcal{M}_{SM}|^2}$. An optimal observable distribution is symmetric for the CP-even Higgs boson and becomes asymmetric when contributions from a CP-odd BSM couplings are present, as shown in Figure 1.
There are three dimension six operators with BSM CP-odd couplings in the SMEFT Lagrangian which can contribute to VBF production or the $H \to ZZ^* \to 4\ell$ decay. Each has an associated Wilson coefficient, which is evaluated in the Warsaw basis. In the present analysis, the optimal observable distributions are used in two ways: the observed distributions are directly used to constrain CP-odd couplings, and in addition they are unfolded to a fiducial phase space, complementing the $H \to ZZ^* \to 4\ell$ differential cross section measurements in Ref. [9], to allow reinterpretations in different models. Since the present search is looking for a distinct CP-odd signature, the extraction of the CP-odd coupling constraints is based only on the shape of the optimal observable distributions, ignoring the expected change in cross section. For VBF production, extracting the differential optimal observable distributions in a VBF-enriched fiducial phase space, rather than the $H \to ZZ^* \to 4\ell$ fiducial phase of [9], would improve the sensitivity to CP violating effects, however this is not yet within statistical reach. Instead this analysis performed an inclusive

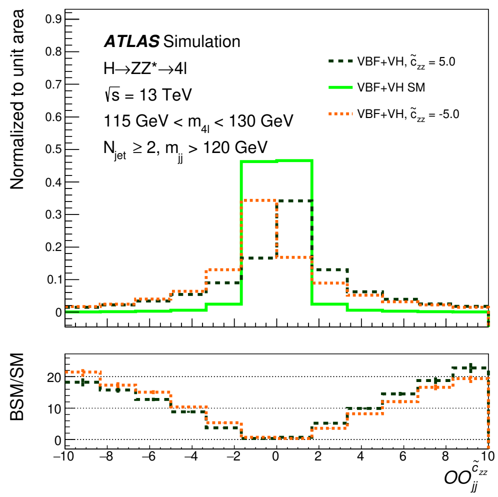


Figure 1: Expected distributions of $OO^{\widetilde{c}_{zz}}_{jj}$ observable for VBF-produced Higgs boson candidates combining the production four signal regions for the SM and for BSM coupling parameter values of $\widetilde{c}_{zz}= -5, 5$. The lower panel shows the ratio of the BSM to SM optimal observable distributions.

cross section measurement in a VBF fiducial phase space. This measurement can be used to constrain BSM models affecting the Higgs boson to ZZ* vertex through their expected impact on event rates.

In Figure 2 on the left, the observed NLL distributions are shown for $c_{H\widetilde{W}}$ for production, decay and their combination, as well as the observed distribution for the combination. The observed differential cross section for the decay optimal observables $OO^{c_{H\widetilde{W}}}_{4\ell}$ is shown in Figure 2 on the right. Figure 3 summarize the expected and observed confidence intervals at 68% and 95% CL for the CP-odd Wilson coefficients. The limits for the Higgs-basis Wilson coupling $\widetilde{c}_{zz}$ are from a production-only observable fit. Those for the coupling $c_{H\widetilde{W}}$ are from a combined-observable fit as this coupling has sensitivity in both production and decay. The rest of the couplings are from a decay-only observable fit, having little sensitivity to the VBF production.

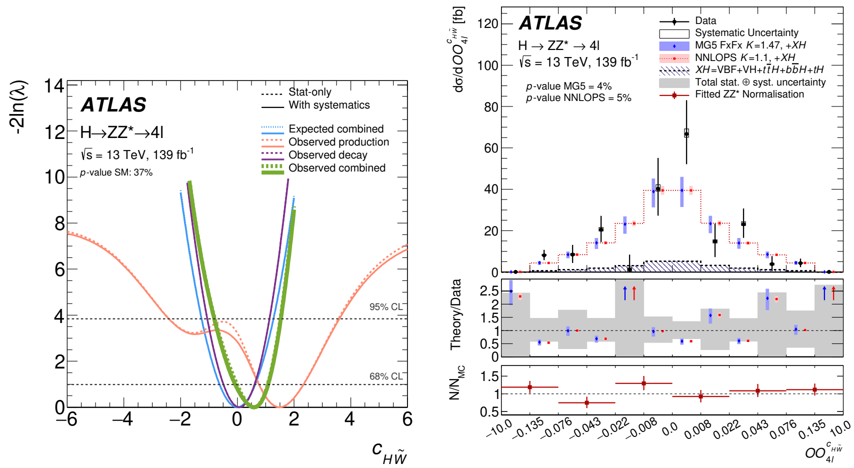


Figure 2: *On the left*: the observed NLL scans as a function of $c_{H\widetilde{W}}$ for production-only $OO_{jj}^{c_{H\widetilde{W}}}$, decay-only $OO_{4\ell}^{c_{H\widetilde{W}}}$ and combined fits. *On the right*: results for differential fiducial cross section for $OO_{4\ell}^{c_{H\widetilde{W}}}$

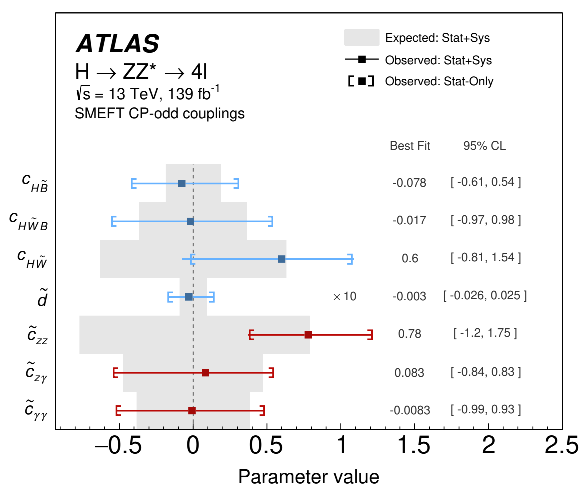


Figure 3: The expected and observed confidence intervals at 68% and 95% CL for the CP-odd Wilson coefficients for an integrated luminosity of 139 $fb^{-1}$ at $\sqrt{s}$=13 TeV.

### 3.2 Combination of the Run 2 and Run 1 Higgs boson mass measurements with the $H \to ZZ^* \to 4l$ the $H \to \gamma\gamma$ channels [2]

The observation of a Higgs boson by the ATLAS [4] and CMS experiments [5] with the Large Hadron Collider (LHC) Run 1 proton-proton (pp) collision data at centre-of-mass energies of s = 7 and 8 TeV was a major step towards understanding the mechanism of electroweak (EW) symmetry breaking. The mass of the Higgs boson was measured to be 125.09 ± 0.24 GeV [10] based on the combined Run 1 data samples of the ATLAS and CMS experiments.
The ATLAS Collaboration measured the Higgs boson mass in the $H \to ZZ^* \to 4\ell$ channel using 139 fb$^{-1}$ of 13 TeV pp collision data [11]. The measured value of the mass is 124.99±0.18(stat.)±0.04(syst.) GeV and is based on improved momentum-scale calibration for muons relative to previous publications. The measurement also employs an analytic model that takes into account the invariant-mass resolution of the four-lepton system on a per-event basis and the output of a deep neural network discriminating signal from background events. This measurement is combined with the corresponding measurement using 7 and 8 TeV proton-proton collision data, resulting in a Higgs boson mass measurement of 124.94±0.17(stat.)±0.03(syst.) GeV. The Higgs boson mass has been measured also in the $H \to \gamma\gamma$ channel using the full Run 2 dataset, and the measured value is 125.17±0.11(stat.)±0.09 (syst.) GeV. The reduction of the uncertainties on the photon energy scale arises from an improved understanding of the difference in data and simulation of the inputs to the photon energy scale regression, and of the introduction of transverse energy ($E_T$) dependent in-situ scales derived from $Z \to e^+e^-$ events, that reduce the calibration extrapolation uncertainties from the $Z$ boson mass to the Higgs mass and from electrons to photons. For this reason, the ATLAS collaboration performed the combination of the Higgs mass measurement with 140 fb$^{-1}$ of 13 TeV between the $H \to ZZ^* \to 4l$ the $H \to \gamma\gamma$, combining also with Run 1 data.
The mass combination is based on the profile likelihood ratio defined in terms of $m_H$, while treating the signal strengths $\mu_i$ as independent parameters

$$\Lambda = \frac{L(m_H, \hat{\hat{\mu}}_i(m_H), \hat{\hat{\theta}}(m_H))}{L(\hat{m}_H, \hat{\mu}_i(m_H), \hat{\theta}(m_H))} \tag{1}$$

The leading source of systematic uncertainty in the mass measurement comes from the energy-momentum scale uncertainties of the main physics objects used in the two analyses, namely muons and electrons for the $H \to 4\ell$ and photons for the $H \to \gamma\gamma$ final states, respectively. They are provided by the E-gamma and Muon combined Performance groups and described in details in the support note of the HZZ and HGam analyses. They also introduces a very tiny correlation between the two measurements.
The results are presented in Figure 4.

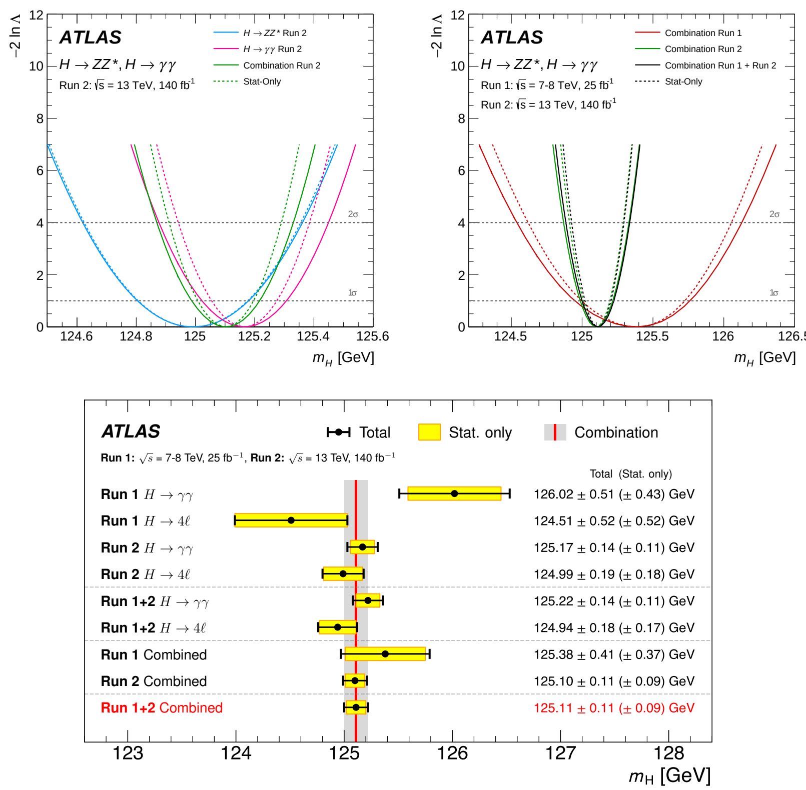


Figure 4: (On the top) The profile likelihood ratio $-2\ln\Lambda$ as a function of $m_H$ for the individual $H \to \gamma\gamma$ and $H \to 4\ell$ channels and their combination using Run2 data only (left), and for Run 1 and Run 2 and their combination (right). The signal strengths are allowed to vary independently. The dashed lines show the statistical components of the mass measurement. (On the bottom) Summary of the $m_H$ measurements from the individual channels and their combination.

### 3.3 Early Run 3 Higgs boson cross section measurement in the he $H \to ZZ^* \to 4l$ decay channel at 13.6 TeV centre-of-mass energy and combination with $H \to \gamma\gamma$ [3]

The Higgs boson decay to four leptons,$H \to ZZ^* \to 4\ell$ where $\ell = \mu, e$, provides good sensitivity for the measurement of its properties due to its high signal-to-background ratio (S/B), which is about 2 for each of the four final states: $\mu^+\mu^-\mu^+\mu^-$ ($4\mu$), $e^+e^-\mu^+\mu^-$ ($2e2\mu$), $\mu^+\mu^-e^+e^-$ ($2\mu 2e$), $e^+e^-e^+e^-$ ($4e$), where the first lepton pair is defined to be the one with the dilepton invariant mass closest to the Z boson mass. The largest background for this channel at the Higgs boson mass, and at higher mass when searching for an additional heavy Higgs boson, is due to continuum $(Z^*/\gamma^*)(Z^*/\gamma^*)$ production, referred to as $ZZ^*$. For the four-lepton events with an invariant mass $m_{4\ell}$ below about 160 GeV there are also non-negligible background contributions from $Z + jets$ and $t\bar{t}$ production with two prompt leptons, where the additional charged lepton candidates arise from decays of hadrons with b- or c-quark content, from photon conversions or from misidentification of jets. With the LHC Run 2 data, collected at centre-of-mass energies of $\sqrt{s} = 13$ TeV, several measurements were performed in the $H \to ZZ^* \to 4\ell$ channel: coupling and spin/CP measurements, cross section measurements, mass and width measurements, and a search for BSM effects. The LHC Run 3 started in 2022 and provided collisions at $\sqrt{s} = 13.6$ TeV. At this energy, the SM Higgs boson production cross section is expected to increase of about 10% relative to $\sqrt{s} = 13$ TeV. This analysis presents preliminary ATLAS fiducial and total Higgs boson production cross sections measurements for the $H \to ZZ^* \to 4\ell$ decay mode using a data sample corresponding to an integrated luminosity of 30.7 fb$^{-1}$ at $\sqrt{s} = 13.6$ TeV.

#### Event Selection

Electrons and Muons are required to pass a *loose* identification criteria and have $E_T > 7$ GeV and $|\eta| < 2.47$ for electrons and $p_T > 5$ GeV and $|\eta| < 2.5$ for muons.

Higgs boson candidates are formed by selecting two same-flavour, opposite-sign lepton pairs (a lepton quadruplet) in an event. The same-flavour opposite-charge lepton pair with the mass closest to the $Z$ boson mass is the leading di-lepton pair $m_{12}$ and is required to be in the range 50 GeV$< m_{12} < 106$ GeV . The sub-leading pair is chosen from the remaining leptons with the invariant mass $m_{34}$ closest to the $Z$, 12 GeV$< m_{34} < 115$ GeV. The four leptons produced are ordered in $p_T$, from the highest to the lowest: $> 20, 15, 10, 5$ GeV. All possible same-flavour opposite-charge di-lepton combinations in the quadruplet must satisfy $m_{4l} > 5$ GeV to remove events containing $J/\psi \to ll$.

Requirements on the impact parameter are applied to reject cosmic rays and to select leptons from primary vertex. Additional studies are on-going to validate the current modelling of the vertex and to study possible improvement on the selection. Indeed currently, to cope with the increase of the reducible background, the four leptons are required to be within the same vertex, applying a selection on the $\chi^2$ of the vertex. This cut could be replaced with a different selection on the impact parameters, that could remove more background and it is also a more natural way to tackle the pile-up background. Finally, the leptons are required to be isolated. The isolation requirements are used in order to select signal events and reject backgrounds. Different isolation working point are provided by the MCP and EGamma performance groups, which have been optimised to have a good signal efficiency and an effective background rejection power.

**Background estimation**

Non-resonant SM $(Z^{(*)}/\gamma^*)(Z^{(*)}/\gamma^*)$ production via $q\bar{q}$ annihilation and gluon–gluon fusion, referred to as $ZZ^*$, can result in four prompt leptons in the final state and constitutes the largest background for this analysis. The normalisation is constrained with a data-driven technique, extending the mass interval considered from 115-130 GeV to 105-160 GeV. The systematic uncertainty is reduced because both the theoretical and luminosity uncertainties no longer contribute to the normalisation uncertainty. The increased mass interval allows an estimation of this process with minimal impact on the expected sensitivity for the signal process. For the fiducial cross section measurement, this contribution is determined as part of the $4\ell$ mass fit in the full four-lepton mass region 105-160 GeV, with the shape of the background taken from simulation.
Other background processes, such as $Z + jets$, $t\bar{t}$, and $WZ$, contain at least one jet, photon or lepton from a hadron decay that is misidentified as a prompt lepton. These reducible backgrounds are significantly smaller than the non-resonant $ZZ^*$ background and are estimated using data where possible, following slightly different approaches for the $\ell\ell\mu\mu$ and $\ell\ell ee$ final states. In the $\ell\ell\mu\mu$ final states, the normalisations for the $Z + jets$ and $t\bar{t}$ backgrounds are determined by performing fits to the invariant mass of the leading lepton pair in dedicated independent control regions which target each background process. Transfer factors to extrapolate from the control regions to the signal region are obtained separately for $t\bar{t}$ and $Z + jets$ using simulation. The $m_{4\ell}$ shape for both processes in each bin is obtained from simulation. The $\ell\ell ee$ control-region selection requires the electrons in the subleading lepton pair to have the same charge, and relaxes the identification, impact parameter and isolation requirements on the electron candidate with the lowest transverse energy. This electron candidate, denoted by $X$, can be a light-flavour jet, an electron from photon conversion or an electron from heavy-flavour hadron decay. Both the extraction of the global yield in the control region and the extrapolation to the signal mass region are performed in bins of the transverse momentum of the electron candidate. Additional contributions from rare processes, such as $tXX$ ($t\bar{t}Z$, $t\bar{t}W$, $tWZ$ and other rare top-associated

processes) and $VVV$ are estimated from simulation.

### Cross section measurement

The total cross section is defined as:

$$\sigma^{\text{tot}} = \frac{N_s}{\varepsilon_{\text{tot}} \cdot BR \cdot \mathcal{L}_{\text{int}}} \ , \tag{2}$$

where BR is the branching ratio of the $H \to ZZ^* \to 4\ell$ final state, $N_s$ is the number of observed signal events, $\mathcal{L}_{\text{int}}$ is the integrated luminosity, $\varepsilon_{\text{tot}}$ is the efficiency for detecting signal, taking into account for trigger, reconstruction and identification efficiencies. This parameter is very model-dependent quantity since it takes into account events which are outside the detector acceptance. Then the total cross section is a measurement extrapolated to regions of phase space in which the detector has no sensitivity. This model dependency can be removed factorising out the acceptance from the definition of the detector efficiency: $\varepsilon_{\text{tot}} = \mathcal{A} \cdot \varepsilon_{\text{fid}}$, where $\mathcal{A}$ is the fiducial acceptance and $\varepsilon_{\text{fid}}$ the fiducial efficiency. In this way the fiducial cross section can be defined as:

$$\sigma^{\text{fid}} = \sigma^{\text{tot}} \cdot \mathcal{A} \cdot BR = \frac{N_s}{\varepsilon_{\text{fid}} \cdot \mathcal{L}_{\text{int}}} \ . \tag{3}$$

The fiducial phase space is defined closely to the selection cuts used in reconstruction of the Higgs boson decays to four lepton. The signal is unfolded at particle-level using the matrix inversion method. This method allows to correct for detector efficiency and resolution taking into account of migration effects between the bins of the distributions.
The cross sections in each final states for the inclusive analysis, are measured performing a binned fit to the $m_{4\ell}$ distribution to extract the number of signal events. The contribution of the non-resonant $ZZ^*$ background is estimated by introducing a floating $ZZ^*$ normalisation, which is fitted simultaneously with the signal in an extended mass window of $105 < m_{4\ell} < 160$ GeV.
The value of the fiducial cross-section is measured to be $\sigma_{fid}$ = 2.80±0.70 (stat.)±0.21 (syst.) fb and is in agreement with the SM prediction of $\sigma_{fid,SM}$ = 3.67±0.19 fb. Figure 5 shows the expected (post-fit) and observed (data) four-lepton invariant mass distribution.

### Combined total cross section measurement between $H \to ZZ* \to 4\ell$ and $H \to \gamma\gamma$

Assuming SM values for the fiducial acceptances and for the branching fractions of the two channels, the fiducial measurements are extrapolated to the full phase space. When performing the extrapolation to the full phase space, additional uncertainties in the acceptance and in the branching fraction are considered. The total Higgs boson production cross-section at 13.6 TeV is measured to be $\sigma(pp \to H)$=67+12 pb using the $H \to \gamma\gamma$ channel and $\sigma(pp \to H)$=46±12 pb using $H \to ZZ* \to 4\ell$ channel. The two measurements

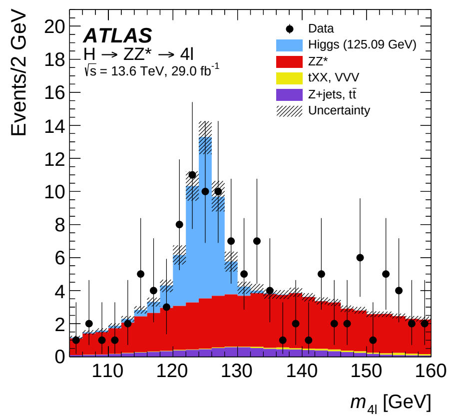


Figure 5: Expected (post-fit) and observed (data) four-lepton invariant mass distribution.

are compatible with a p-value of 20%. The total Higgs boson production cross-section, obtained by combining the $H \to ZZ* \to 4\ell$ and $H \to \gamma\gamma$ results, is 58.2±8.7 = 58.2±7.5 (stat.)±4.5 (syst.) pb at 13.6 TeV.
The values of the total cross-section determined from this analysis, and those from previously published ATLAS studies, are shown in Figure 6 as a function of the $pp$ centre-of-mass energy. The measurements at the new centre-of-mass energy of 13.6 TeV are in good agreement with the SM prediction.

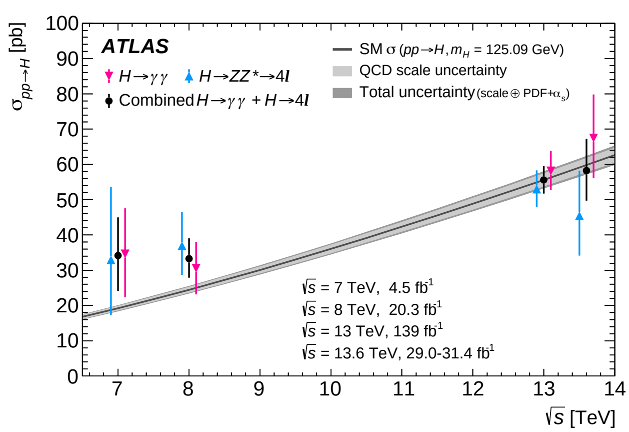


Figure 6: Values of the Higgs boson production cross section measurements from this and previous ATLAS publications as a function of the pp centre-of-mass energy. The SM predicted values and their uncertainties are shown by the shaded band. The individual channel results are offset along the x-axis for display purposes.

## 3.4 Higgs boson properties measurement at 13.6 TeV with coming data

Moving forward to the new data coming from the entire Run 3 data taking phase for ATLAS, the efforts are focused on building the analyses frameworks and strategies to provide new Higgs boson properties measurements at 13.6 TeV.

### $H \to \mu\mu$ decay channel

The search in this decay channel just started aiming to provide a new measurement of the signal strength in this channel that can be combined with the full Run 2 dataset. This will help to improve the sensitivity in this very rare Higgs boson decay channel. Several studies are on-going to improve the sensitivity: improve the VBF categorisation and study alternative observables to extract the signal, improving the vertex reconstruction and the background modelling.

### $H \to 4\ell$ differential cross section measurement and STXS

With the increased statistics of about 56 $\text{fb}^{-1}$ with respect to the early Run3 analysis, the plan is to provide more granular cross section information both at decay side (differential) than at production side (STXS). Preliminary studies already started aiming to define the analysis baseline for all the future Run3 analysis. Figure 7 shows the expected differential cross section distribution for the Higgs boson transverse momentum and for the number of jets at 13.6 TeV with an integrated luminosity of 56 $\text{fb}^{-1}$.

Both those approaches can be interpreted to put constraint on anomalous Higgs boson couplings. In particular, the STXS results can interpreted in what is called $\kappa$-framework, putting constraints on the anomalous couplings with vector bosons $\kappa_V$ and fermions $\kappa_F$. Given that the statistics is still far away from what was expected and what was the Run2 goal, the plan is to combine the results on $\kappa_V$,$\kappa_F$ with the one obtained in Run2 and get more stringent limits.

**Responsabilities:**

- Chiara Arcangeletti: convener of the Higgs subgroup $HZZ$
- Chiara Arcangeletti: Contact Editor of the "*Test of CP-invariance of the Higgs boson in Vector Boson Production and its decay to Four Leptons*" paper
- Chiara Arcangeletti: Analysis Contact of the "*Combination of the Run 2 and Run 1 Higgs boson mass measurements with the $H \to ZZ^* \to 4l$ the $H \to \gamma\gamma$ channels*" analysis

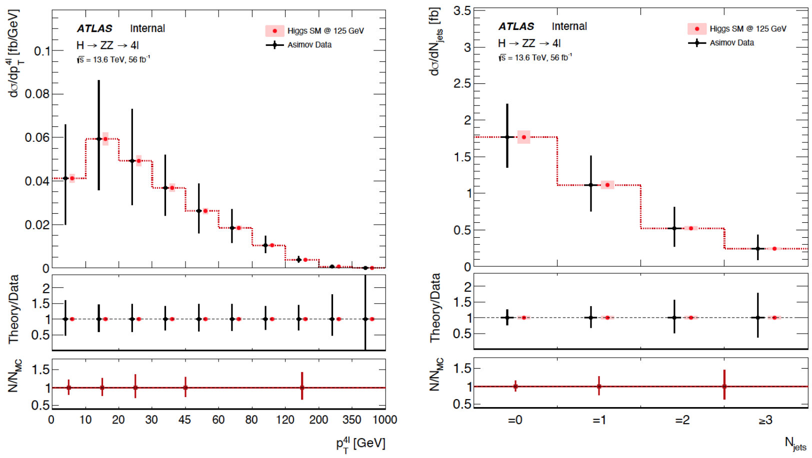


Figure 7: Expected differential cross section measurements for the Higgs boson transverse momentum and for the number of jets at 13.6 TeV with an integrated luminosity of 56 fb$^{-1}$

- Chiara Arcangeletti: Analysis Contact of the "*Early Run 3 Higgs boson cross section measurement in the he $H \to ZZ^* \to 4l$ decay channel at 13.6 TeV centre-of-mass energy*" analysis

**Talks at conferences:**

- Chiara Arcangeletti: *Measurement of Higgs boson production and search for new resonances in final states with photons and Z bosons with the ATLAS detector*, LHC Seminar, CERN (Geneva), 6th June 2023 (Invited Speaker)
- Chiara Arcangeletti: *Measurement of Higgs boson production and properties*, LHCP 2023, 11th Large Hadron Collider Physics Conference, Belgrade (Serbia), 22-26 May 2023 (Speaker on behalf of the ATLAS and CMS Collaborations)
- Chiara Arcangeletti: *Ricerca della violazione di CP nelle interazioni del bosone di Higgs con i bosoni vettori*, IFAE 2023, Incontri di Fisica delle Alte Energie, Catania (Italia),12-14 April 2023 (Speaker)
- G. Mancini: *Summary of ATLAS Higgs Physics*, BSM 2023, Hurgada (Egypt) 6-9 November (Speaker)

## References


[1] G. Aad *et al.* [ATLAS], "Test of CP-invariance of the Higgs boson in vector-boson fusion production and its decay into four leptons," [arXiv:2304.09612 [hep-ex]].

[2] G. Aad *et al.* [ATLAS], "Combined measurement of the Higgs boson mass from the $H \to \gamma\gamma$ and $H \to ZZ^* \to 4\ell$ decay channels with the ATLAS detector using $\sqrt{s} = 7$, 8 and 13 TeV *pp* collision data," Phys. Rev. Lett. **131** (2023), 251802 doi:10.1103/PhysRevLett.131.251802 [arXiv:2308.04775 [hep-ex]].

[3] G. Aad *et al.* [ATLAS], "Measurement of the $H \to \gamma\gamma$ and $H \to ZZ^* \to 4\ell$ cross-sections in pp collisions at $\sqrt{s} = 13.6$ TeV with the ATLAS detector," Eur. Phys. J. C **84** (2024) no.1, 78 doi:10.1140/epjc/s10052-023-12130-5 [arXiv:2306.11379 [hep-ex]].

[4] G. Aad *et al.* [ATLAS], "Observation of a new particle in the search for the Standard Model Higgs boson with the ATLAS detector at the LHC," Phys. Lett. B **716**, 1-29 (2012) doi:10.1016/j.physletb.2012.08.020 [arXiv:1207.7214 [hep-ex]].

[5] S. Chatrchyan *et al.* [CMS], "Observation of a New Boson at a Mass of 125 GeV with the CMS Experiment at the LHC," Phys. Lett. B **716**, 30-61 (2012) doi:10.1016/j.physletb.2012.08.021 [arXiv:1207.7235 [hep-ex]].

[6] G. Aad *et al.* [ATLAS], "Higgs boson production cross-section measurements and their EFT interpretation in the $4\ell$ decay channel at $\sqrt{s}$ =13 TeV with the ATLAS detector," Eur. Phys. J. C **80**, no.10, 957 (2020) [erratum: Eur. Phys. J. C **81**, no.1, 29 (2021); erratum: Eur. Phys. J. C **81**, no.5, 398 (2021)] doi:10.1140/epjc/s10052-020-8227-9 [arXiv:2004.03447 [hep-ex]].

[7] M. Diehl and O. Nachtmann, "Optimal observables for measuring three gauge boson couplings in e+ e- —> W+ W-," [arXiv:hep-ph/9603207 [hep-ph]].

[8] I. Brivio and M. Trott, "The Standard Model as an Effective Field Theory," Phys. Rept. **793**, 1-98 (2019) doi:10.1016/j.physrep.2018.11.002 [arXiv:1706.08945 [hep-ph]].

[9] G. Aad *et al.* [ATLAS], "Measurements of the Higgs boson inclusive and differential fiducial cross-sections in the diphoton decay channel with pp collisions at $\sqrt{s} = 13$ TeV with the ATLAS detector," JHEP **08**, 027 (2022) doi:10.1007/JHEP08(2022)027 [arXiv:2202.00487 [hep-ex]].

[10] G. Aad *et al.* [ATLAS and CMS], "Combined Measurement of the Higgs Boson Mass in *pp* Collisions at $\sqrt{s} = 7$ and 8 TeV with the ATLAS and

CMS Experiments," Phys. Rev. Lett. **114**, 191803 (2015) doi:10.1103/PhysRevLett.114.191803 [arXiv:1503.07589 [hep-ex]].

[11] [ATLAS], "Measurement of the Higgs boson mass in the $H \to ZZ^* \to 4\ell$ decay channel using 139 fb$^{-1}$ of $\sqrt{s} = 13$ TeV $pp$ collisions recorded by the ATLAS detector at the LHC," [arXiv:2207.00320 [hep-ex]].

# 4 Upgrade of the forward Muon Spectrometer for ATLAS using frontier MPGD (MicroPatternGasDetector) detectors such as MicroMegas.

ATLAS [1] (Figure 8 (left)) is one of the main experiments at the Large Hadron Collider (LHC) [2] and is undergoing the phase 1 upgrade in order to cope with the higher luminosity foreseen for the future LHC Runs. The old Small Wheels were the first muon spectrometer station in the forward region (End-Cap) with an angular coverage in pseudorapidity of $1.3 < |\eta| < 2.7$ and were composed by Cathode Strip Chambers and Monitored Drift Tubes. An improvement in the performances was required in the NSW ([3]) both for the trigger and the track reconstruction in view of the increasing luminosity of LHC ($5 - 7 \times 10^{34}\ cm^{-2}s^{-1}$) to maintain or even improve the performances of the detector.
Micromegas (MM) [4] and small Thin Gap Chambers (sTGCs) were chosen as fast detectors able to perform precision tracking ($\sim 100\ \mu m$ per plane [5] with an efficiency $> 90\%$) and to cope with the increasing background particle flux as the luminosity increases (up to $20\ kHz/cm^2$) while rejecting fake triggers. The ATLAS MM detectors have a trapezoidal shape, to match with the wheel structure of the NSW as shown in Figure 8 (center). Each of the 2 NSWs is composed of 16 sectors: 8 small (SM1 and SM2) and 8 large sectors (LM1 and LM2). The production is distributed between several industries and institutes: Italy (SM1) [6], Germany (SM2), France (LM1), Russia-Greece-CERN (LM2). Each sector of the NSW is a sandwich of 2 sTGC Wedges and a MM Double Wedge as shown in Figure 8 (right). The NSW MM wedges are formed by 2 quadruplet detectors one after the other, type 1 detectors at lower radius and type 2 at larger radius as can be appreciated in Figure 8 (right), with 8 printed circuit boards (PCBs) in total (5 from type 1 modules and 3 for type 2 modules).

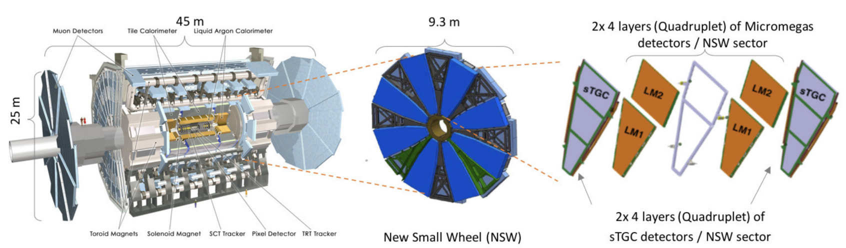


Figure 8: The ATLAS Detector at the LHC (left) showing the position of the NSWs with their sector structure (center) and the composition of each sector out of sTGC and MM quadruplet modules (right).

# 5 Micromegas operating principles and NSW structure

The resistive Micromegas chambers are frontier Micro-Pattern Gas Detectors with a planar geometry as shown in Figure 9 (left) operating in a gas mixture of $Ar : CO_2$ (93%:7%); studies ongoing on a new ternary gas mixture will be presented later. They have a 5 $mm$ conversion (drift) gap, a floating mesh embedded in the drift panel structure and a 128 $\mu m$ wide amplification gap between the read-out (RO) PCBs and the mesh (supported by insulating pillars of millimetric diameter). The PCBs are produced by industries, with 300 $\mu m$ wide strips and a pitch of $425 - 450$ $\mu m$. Resistive strips are superimposed to the copper signal strips to mitigate the intensity of discharges [7]. The detector, in this fashion, is really compact with a high electric field ($\sim$ 45 $kV/cm$) on a surface of $O(m^2)$ in the amplification gap, high transparency and with fast ions evacuation ($\sim 100$ $ns$). NSW MM were

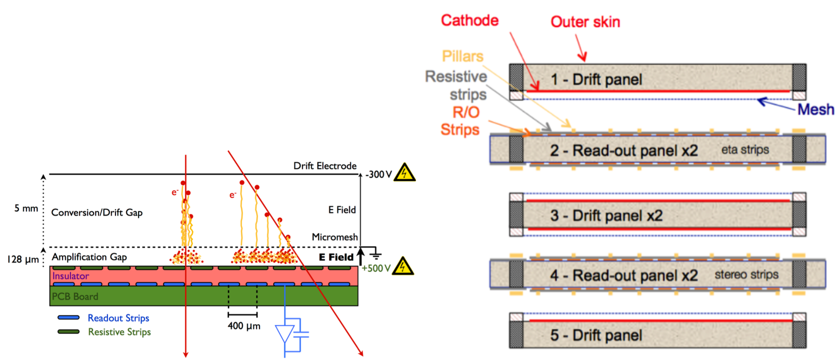


Figure 9: (left) Working principle of a MM chamber (right) MM quadruplet scheme.

produced for the first time on large dimensions ($O(m^2)$) and were constructed with some peculiarities with respect to the status of the art of the pre-esistent MM technology:

- screen printed resistive strips capacitively coupled to copper read-out strips, in order to cope with the high flux expected in view of the HL-LHC future Runs

- mesh at ground potential in order to allow for separation of the anode in separate HV sections, which was required by the fact that industries had limitations in dimensions of the PCBs

- mechanically "floating"mesh, which is integrated in the drift panel structure and not embedded in the anodic structure (as it was for the bulk MM [4]). This is necessary for large area detectors and allows for chamber re-opening in case of intervention.

Each MM chamber is a quadruplet formed by 5 stiff panels needed to form 4 gaps when coupled (Figure 9 (right)): 2 RO panels, and 3 drift panels composed by cathode PCBs and the meshes. Two out of four layers have strips inclided by $\pm 1.5°$ in order to reconstruct the $2^{nd}$ coordinate (stereo layers), while the other two aim for precision coordinate reconstruction (eta layers). The mesh is grounded, the RO resistive strips are at $\sim 570\ V$ and the cathode at $-300\ V$. Resistive strips are screen printed with equidistant interconnections to have uniform resistance across the pcb, with a design resistivity of $\sim 10\ M\Omega/cm$. This peculiar structure of the ATLAS MM allows the detector to be re-opened for intervention since the mesh is not glued on top of the RO panel, and makes an easier construction procedure; each PCB is diveded into 2 HV sections, having in total 40 HV channels for the type 1 ATLAS MM chambers (5 PCBs per layer) and 24 HV channels for the type 2 ones (3 PCBs per layer).

# 6 Underground Commissioning and first results in terms of performances

NSW have been succesfully commissioned at CERN with a strong contribution of our team being involved in all the activities and have been lowered to the ATLAS cavern at the end of 2021.
In May-July 2022 first Splashes were driven by LHC and current has been observed by the NSW. In Figure 10(left) we can appreciate the current from one sector of the MM NSWs which is following nicely the luminosity driven by LHC and a nice event display involving the NSW System.
This was followed by the first Runs in Autumn, for which we do have similar impressive results (Figure 10).

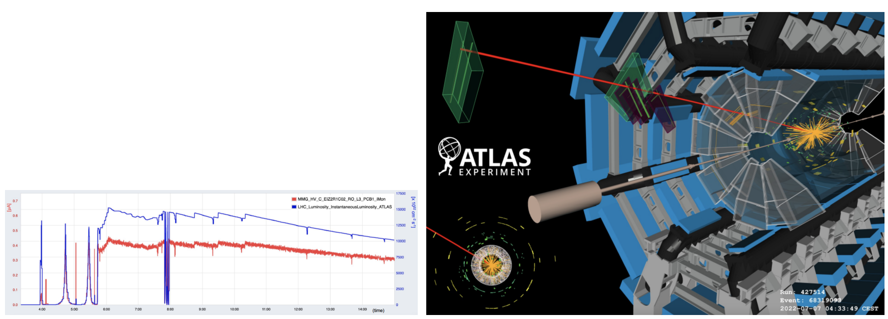


Figure 10: (left) Current of MM detectors during early Run3 Runs (right) Event display involving the NSW.

Commissioning undergroung proceeded and we are currently running at 505 V in the ternary gas mixture ($Ar : CO_2 : Iso$ 93 : 5 : 2) with less than 1% of channels not at nominal HV and around 1.5% of HV channels disconnected or

disabled (including 1 drift channel). As from now, we still have margin to push the amplification higher.
Operation has been done by our team in order to try to recover HV bad section with the Argon curing procedure (developed by our team together with Rui De Olivera at CERN). With this procedure we managed to recover 60% of the HV channels treated, which is a huge and promising achievement. An example of the Argon curing performed is shown in Figure 11.


Figure 11: Example of Argon Curing on a sector.

## 7 First results

A great effort has been put on understanding the DAQ instabilities found on the NSW system and in 2023 we managed to achieve a very constant behaviour in terms on acquisition stability with efficiencies ranging from 70 95% on average. The situation is much more improved with respect to the 2022 preliminary results and was mainly drawn by DAQ issues (as shown in Figure 12), but there is still room for improvements.

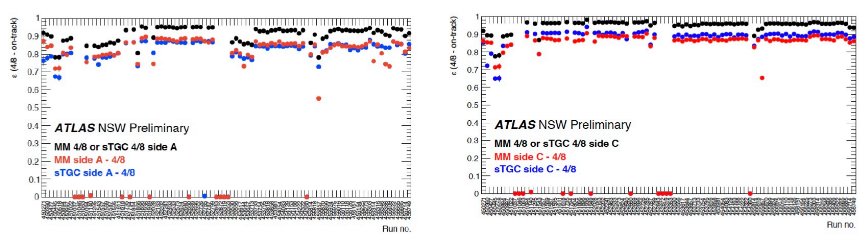


Figure 12: Acquisition stability in time.

The layer by layer efficiency with cluster selected within $\pm$ 5 $mm$ with respect to the extrapolated track position have been studied, including all inefficiencies (detector, HW, DAQ). In Figure 13, the results obtained for the Wheel A are reported as an example.

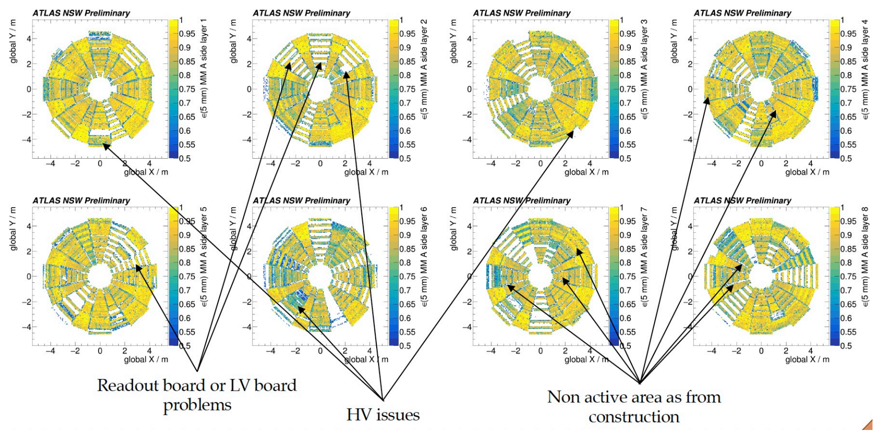


Figure 13: Layer efficiency for Wheel A (including detector, HW and DAQ inefficiencies).

Thanks to this results, the track reconstruction with clusters associated to the muon track, the on-track efficiency with at least 4/8 detector layers allows to achieve a track reconstruction > 95% thanks to the high-redundancy of the NSW, as shown in Figure 14.

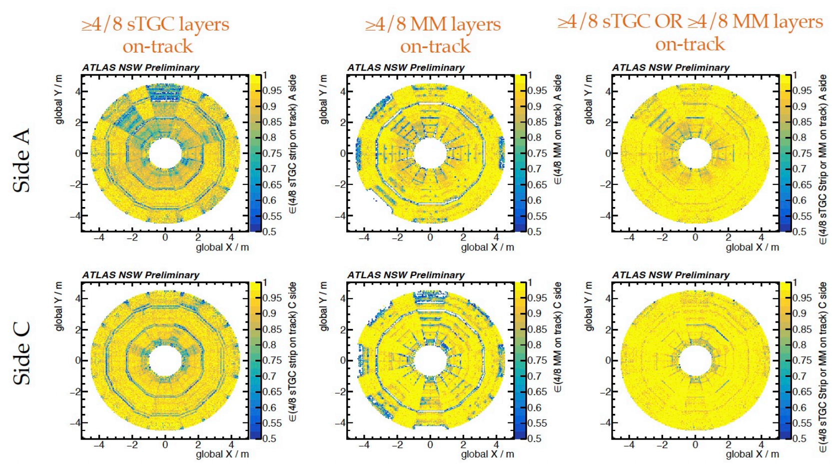


Figure 14: Track reconstruction efficiency.

As for the Level-1 trigger, NSW requirements have been designed targeting the requirements imposed by the HL-LHC running conditions, exploding the full potential of the NSW trigger for HL-LHC Runs. As from the actual status, the NSW has been already included in the L1 trigger decision, leading to a rate reduction of 6 $kHz$ as shown in Figure 15.

**Responsabilities:**

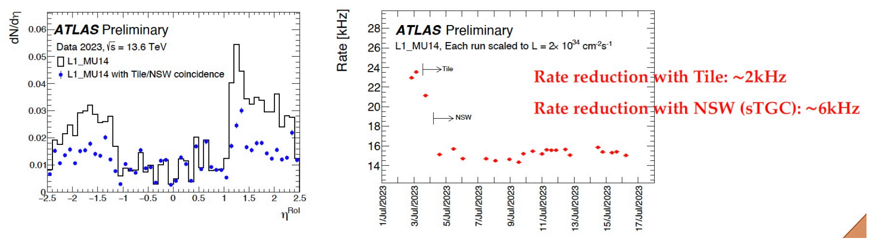


Figure 15: ATLAS Level 1 trigger rate with Tile and NSW.

- Mario Antonelli NSW Project Leader
- Giada Mancini On Call Expert for MM
- Chiara Argangeletti On Call Expert for MM

**Talks at conferences:**

- G. Mancini: TeVPA2023 Conference Talk ”Performance studies of Micromegas detectors in ATLAS with Run3 data”
- G. Mancini: PIC2023 Conference Talk ”Performance studies of Micromegas detectors in ATLAS with Run3 data”

# References


[1] ATLAS Collaboration, 2008 JINST 3 S08003

[2] Lyndon Evans and Philip Bryant, LHC Machine, JINST 3 (2008) S08001

[3] ATLAS collaboration, New Small Wheel Technical Design Report, CERN-LHCC-2013-006 (2013)

[4] Y. Giomataris, P. Rebourgeard, J. Robert and G. Charpak, A High granularity position sensitive gaseous detector for high particle flux environments, NIM A 376 (1996) 29

[5] A. Koulouris et al., ATLAS New Small Wheel Micromegas production and performance, NIM A 958 (2020) 162757

[6] T. Alexopoulos et al., Construction techniques and performances of a full-size prototype Micromegas chamber for the ATLAS muon spectrometer upgrade, NIM A 955 (2020) 162086

[7] T. Alexopoulos et al., A spark-resistant bulk-micromegas chamber for high-rate applications, NIM A 640 (2011) 110-118

# 8 Muon Phase 2

## 8.1 MUON Detector Control System

The MUON Detector Control System (DCS) involvement, tasks, projects and requirements will be summarised in this document. The day to day tasks are the refactoring/restructuring of large-code based projects, hardware/ software testing, integration and also provide interface and services that are critical during daily operation and readiness of the distributed control systems.
The coordination for the ATLAS MUON Collaboration Control Systems required the supervision, release management and debugging of the active projects of the MUON DCS group. Maintenance and Operation of the system during 2023 Run period was of vital importance for the systems.
New Small Wheel (NSW) as a specific relatively new system needed further development of the real time software applications which include Power Supply systems, Electronics monitoring, Environmental parameters, Gas monitoring and Beam Injection/ Permit system. Finally during migration and problem solving, collaborating with the CERN groups of ATLAS Central DCS and BE/ICS for centrally released framework tools and OPC UA/DA server interfaces that are integrated to MUON DCS systems during issue investigation or integration and debugging of the control software after system migrations (Alma 9/WinCCOA 3.19). Already existing projects had to be developed/altered.
Particularly the common Muon hardware of the Beam Injection System (BIS) which is dominated by an Agilent module and actuator switches to provide the Injection Permit, Automatic High Voltage transition and control of the Reset Network needs replacement.
The BIS is currently used to receive the Stable Beams flag while operating seemingly with the DCS to automatically bring the sub detector systems to the desired state, it sends the Injection Permit flag between the MUON subsystems and also can reset the various mainframes, controllers and Racks. However the current system is limited in terms of granularity and specifications since the NSW was integrated to the old BIS, however the needs of the system are demanding in such a way that many functions are absent in the NSW but in legacy systems as well. New hardware specifications and improved DCS will allow the NSW to acquire the desired granularity, functionality and meet the actual requirements.
The new System was reviewed during 2023 and hardware passed the Final Design Review however the software needs further development to include all the possible functionalities and further increase the granularity of the systems. The last project includes the unification of the DCS of the Muon collaboration Power supply System. In View of Phase-II upgrade, which will conclude the process of adapting the MUON spectrometer to the needs of HL- LHC increased integrated luminosity, started with Phase-I upgrade of NSW, the legacy power supply system has to be replaced due to component obsolescence, ageing and radiation damage.

Up to date control protocols, new power systems and backwards compatibility are required thus the current MUON DCS is re-designed in order to be prepared to address such a major upgrade.
Legacy system differences made it practically impossible to use universally, the same types of Hight Voltage and Low Voltage hardware and as such the DCS development diverged.
The project of the DCS unification of the legacy detectors and the NSW upgrade will have a major impact in the functionality of the MUON spectrometer Power supply systems.
**Responsabilities:**

- Christos Paraskevopoulos: Coordination of the ATLAS MUON Collaboration Detector Control System at CERN. Development, maintenance, operation and release management. Review and design of new Interfaces and applications for the system upgrades.

- Christos Paraskevopoulos: Coordination of the NSW Detector Control System. Developer/Researcher, focused on the design and development of Automated Industrial software, hardware testing and commissioning for distributed Control systems, Finite State Machine design and development for power supply systems, environmental parameters monitoring, Beam Injection systems and Automatic procedures (control, monitor, procedures, archiving, alert handling, data analysis). Testing of the hardware setup and project deployment equipped with different type of devices/sensors for the commissioning and integration to the ATLAS experiment.

# 9 Inner Tracker (ITk) for Phase-II upgrade

After the Phase-I upgrade, the LHC will undergo a Phase-II upgrade, to deliver the instantaneous luminosity of $\sim 7.5 \times 10^{34} cm^{-2} s^{-1}$, more than a factor 10 beyond its design value, corresponding to unprecedented pile-up conditions with an a average of 200 interactions per crossing. The ATLAS detector will be upgraded to maintain its capabilities. In particular the Inner Detector, with acceptance up to $|\eta| < 2.5$, will be substituted by a new, all-silicon Inner Tracker (ITk), whose acceptance will be $|\eta| < 4.0$. The ITk detector comprises two subsystems: a Strip Detector surrounding a Pixel Detector. The ITk layout is shown in Fig.16, left. The Strip Detector (blue), covering $|\eta|$ <2.7, is complemented by a 5 layer Pixel Detector (red) extending the coverage to $|\eta| < 4$. LNF is involved in the construction of one outer pixel endcap of the ITk and in simulation of the performance of the reconstruction of jets and the missing transverse energy.

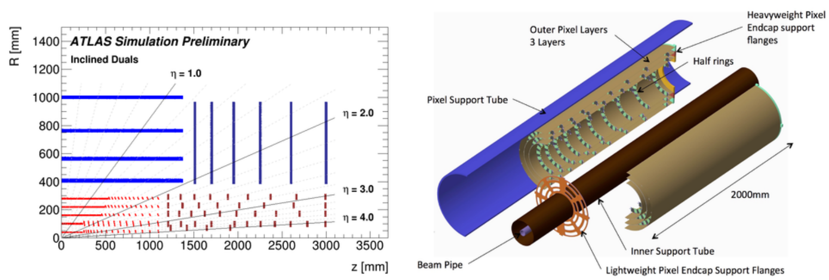


Figure 16: Left: Schematic layout of the ITk. The barrel and endcap for the pixel and strip sub-systems are shown in red and blue respectively. The rings of the pixel endcap are shown as red vertical lines. Right: Exploded 3D drawing of one Outer End-cap.

## 9.1 ITk outer-endcap construction

LNF is responsible of the construction of one outer endcap of the ITk Pixel detector. The pixel end-cap system is designed to supply a minimum of at least 9 hits from the end of the strip coverage in pseudorapidity to $|\eta| = 4$. The novel concept is the end-cap ring system, where layers of pixel rings extend the coverage in $z$ and allow routing of the service separately along each ring layer. More information is in [1]. A 3D model of one outer endcap is shown in Fig.16, right. Each layer of rings is supported by a 0.6mm carbon fiber cylinder "shell", along which services for the rings are routed. Each ring is constructed from two half-rings, each covering just over half of the $\phi$ coverage of the entire ring. The pixel services (cables, cooling pipes, data lines) are routed from their sources out to Pixel Patch-Panel 1 (PP1). LNF is responsible until Q3 of 2024 of the design, prototyping of PP1 mechanical

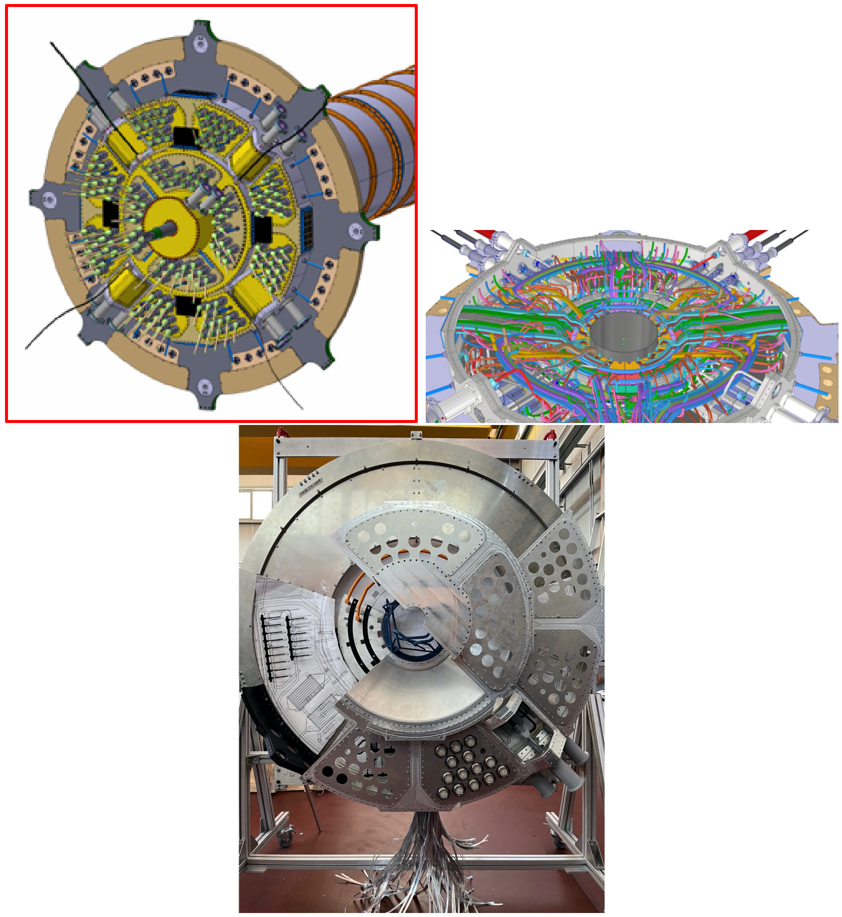

Figure 17: Top Left: overview of the PP1. Top Right: design of cabling and piping system inside the PP1 volume. Bottom: prototype at LNF

structure, as well as the design of the cabling and piping inside the PP1 volume, see Figure 17. The prototype of the PP1 mechanical structure has been constructed under the LNF design from an external company in 2020. A large effort is currently on going to design the complex routing of the services and to manage the space to allow the welding of cooling pipes, as well as the integration procedure and testing of the PP1 at CERN. An extensive activity is on going to populate the PP1 volume with 3D printed pipes and with prototypes cables, to validate the design. A crucial part of the PP1 design is the data cable feed-through. Full scale prototypes have been realized and tested. LNF has the responsibility to design and produce a heaters system on

Figure 18: Top: prototype tool for holding individual half-shell and for mating half-shell pairs. Bottom: merged lines from two local boxes of the $CO_2$ plant at LNF

the external surface of the PP1, needed to prevent condensation when a cooling failure happens. The design of the heater system is mostly finalized. Prototypes have been purchased and successfully tested.
For the ITk endcap assembly at LNF, the tools to hold the individual half-shells, allow the mating of half-shells pair and hold the fully assembled

endcap have been produced, see Fig. 18 top. The part of the tool involving a rotational movement has been constructed by an external company using the LNF design, while the central part of the tool has been constructed in the LNF mechanic workshop and aligned to the requested precision in 2022. A platform for the mechanical assembly of the detector has been designed and produced and it's integrated in the clean room floor. Further tools are needed to move the endcap inside the clean room and for the transport of the endcap to CERN. Their design is on going. LNF contributed to the development and testing of the electrical bundles from the detector to the PP1 connectors. Prototypes have been purchased and tests to check electrical continuity during a thermal cycle have been successfully performed.
LNF is responsible to design and purchase the data-cable extenders to connect the data-cable wrapped on the detector-trolley to the opto-electrical conversion system, for all the ITk pixel subsystems. The order for six bundle prototypes have been placed. A system test activity is on-going to test

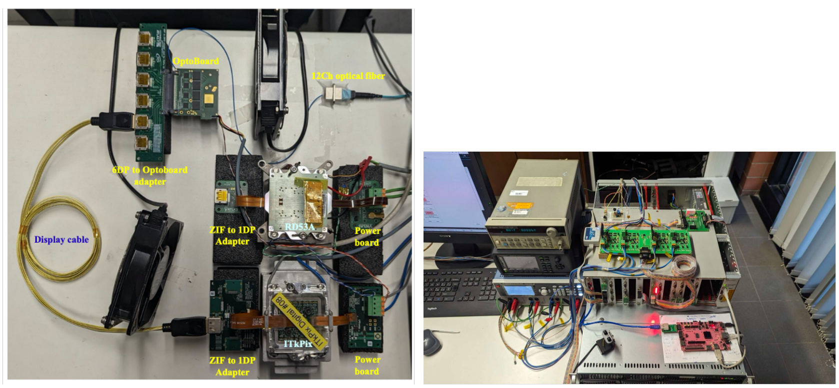


Figure 19: Left: Readout of ITk pixel quad modules through adapter board designed and produced at LNF. Right: interlock system

ITKPix1 quad-modules using the optical readout with the FELIX cards, see Fig. 19 left. Data adapter boards have been designed, tested and produced. They have been spread in the ITk community and are widely used. The interlock crate has been received. The interlock interfaces with the $CO_2$ plant have been developed and commissioned ( Fig. 19 right ). A modular and scalable DCS software development is on going.
Large infrastructures are needed for the testing. A $CO_2$ cooling system with maximal 4kW cooling power will cool-down modules to $\sim$ -20C, through the cooling pipes inside the half-rings. This $CO_2$ cooling system has been constructed by the LNF cryogenic plants service in collaboration with CERN and DESY and NIKHEF institutions and is at LNF. The merging of the cooling lines from the two individual boxes to get the maximum flux of 20 g/s for one user application has been successfully tested, see Fig. 18 bottom. The order for the cooling lines from the plant to the area in the clean room where

the endcap will be tested has been placed.
A large climate chamber with internal dimensions of 3600 mm $\times$ 4000 mm $\times$ 2400 mm (L $\times$ P $\times$ H) has been purchased and is present at LNF Thermal cycling of the final half-shells, loaded with services and half-rings, (half-shell prototypes partially loaded) from -45C to +50C (-55C to +60 C) is foreseen.
The order for additional dry air lines has been placed.
The clean room inside Capannone Gran Sasso is mostly finalized. .
**Publications, internal documents and public presentations:**

- S.Tomassini: several presentations during the ATLAS Upgrade week and ITk week at CERN
- E. Dane': several presentations during the ATLAS Upgrade week and ITk week at CERN
- F. Rosatelli: several presentations during the ATLAS Upgrade week and ITk week at CERN
- Z. Chubinidze, edms document AT2-IP-ER-0066, Design of ERF-6DP adapter card for ITkPix module, report of Qualification Task
- Z. Chubinidze, edms document AT2-IP-ER-0065, Interlock System for EC integration at INFN-LNF, report of Qualification Task
- M. Testa, analysis team of ATLAS Public Note Performance studies of tracking-based triggering using a fast emulation
ATL-DAQ-PUB-2023-001

**Responsibilities in 2023 ATLAS - ITk**

- M. Testa, one pixel endcap integration
- S. Tomassini, up to September 2023 one pixel endcap integration
- S. Tomassini, up to Sep 2023 design and construction of two patch panels 1 (PP1s)
- M. Testa; CERN Pixel System Test coordination
- E. Dane'; piping design inside PP1 volume
- F. Rosatelli; cabling design inside PP1 volume

# References

[1] ATLAS Collaboration, "Technical Design Report for the ATLAS ITk Pixel Detector", CERN-LHCC-2017-021; ATLAS-TDR-030